

## Research Paper

# Polydopamine Nanoparticles as a Versatile Molecular Loading Platform to Enable Imaging-guided Cancer Combination Therapy

Ziliang Dong<sup>1</sup>, Hua Gong<sup>1</sup>, Min Gao<sup>1</sup>, Wenwen Zhu<sup>1</sup>, Xiaoqi Sun<sup>1</sup>, Liangzhu Feng<sup>1</sup>, Tingting Fu<sup>2</sup>, Yonggang Li<sup>2</sup>, Zhuang Liu<sup>1</sup>✉

1. Institute of Functional Nano & Soft Materials (FUNSOM), Collaborative Innovation Center of Suzhou Nano Science and Technology, the Jiangsu Key Laboratory for Carbon-Based Functional Materials & Devices, Soochow University, Suzhou, Jiangsu 215123, China.
2. The First Affiliated Hospital of Soochow University, Suzhou, Jiangsu 215006, China.

✉ Corresponding author: E-mail: zliu@suda.edu.cn.

© Ivyspring International Publisher. Reproduction is permitted for personal, noncommercial use, provided that the article is in whole, unmodified, and properly cited. See <http://ivyspring.com/terms> for terms and conditions.

Received: 2015.11.16; Accepted: 2015.12.25; Published: 2016.04.28

## Abstract

Cancer combination therapy to treat tumors with different therapeutic approaches can efficiently improve treatment efficacy and reduce side effects. Herein, we develop a theranostic nano-platform based on polydopamine (PDA) nanoparticles, which then are exploited as a versatile carrier to allow simultaneous loading of indocyanine green (ICG), doxorubicin (DOX) and manganese ions (PDA-ICG-PEG/DOX(Mn)), to enable imaging-guided chemo & photothermal cancer therapy. In this system, ICG acts as a photothermal agent, which shows red-shifted near-infrared (NIR) absorbance and enhanced photostability compared with free ICG. DOX, a model chemotherapy drug, is then loaded onto the surface of PDA-ICG-PEG with high efficiency. With Mn<sup>2+</sup> ions intrinsically chelated, PDA-ICG-PEG/DOX(Mn) is able to offer contrast under T1-weighted magnetic resonance (MR) imaging. In a mouse tumor model, the MR imaging-guided combined chemo- & photothermal therapy achieves a remarkable synergistic therapeutic effect compared with the respective single treatment modality. This work demonstrates that PDA nanoparticles could serve as a versatile molecular loading platform for MR imaging guided combined chemo- & photothermal therapy with minimal side effects, showing great potential for cancer theranostics.

Key words: Polydopamine, Indocyanine green, Nano-Drug delivery system, Combination therapy, Magnetic resonance imaging.

## Introduction

Chemotherapy, although is a commonly used cancer therapy strategy, has many inevitable problems such as severe side effects [1], limited efficacies, and the possibility to trigger multidrug resistance [2]. Thus, the development of smart nano-drug delivery systems (NDDSs) with excellent tumor-targeting ability and accurately controlled release profile has attracted a great deal of attentions in recent years [3, 4]. Up to now, a large variety of multifunctional nanoplatfoms responsive to various external and/or internal stimuli (e.g. light [5], heat

[6-8], ultrasound [9, 10], magnetic field [11, 12], acidic pH value [13] and redox environment [14]) have been rationally designed and demonstrated to be efficient for cancer therapy with higher efficacy and limited side effects compared to conventional chemotherapy in many pre-clinical animal studies. Among those strategies, photothermal therapy (PTT), which utilizes the heat generated from laser irradiation of near infrared (NIR) light-absorbing agents to kill cancer cells, has been widely explored and showed great synergistic therapeutic effects when applied together

with chemotherapy or other therapeutic modalities [15-17]. Unlike common photothermal therapy strategy by heating to a high temperature (e.g. over 50°C), which kills cancer cells via hyperthermia induced cell necrosis, a mild photothermal heating (43-45°C) without directly causing cell death can efficiently improve chemotherapy efficacy by enhancing the cellular uptake of chemotherapeutics or triggering the intracellular drug release from nanocarriers [6, 18]. Additionally, a number of imaging methods such as fluorescent imaging [19], magnetic resonance imaging [20], and photoacoustic imaging [21, 22], have been integrated with those NDDSs for imaging guided therapy. With the aid of imaging, it would be possible to monitor the behaviors of those NDDSs and then optimize the therapeutic windows, useful for accurate personalized therapy with further improved therapeutic effects and reduced side effects.

To build NIR-triggered nano-drug carriers, many photothermal agents have been extensively explored in recent years. Although a large variety of inorganic nano-agents (e.g. gold nanomaterials, carbon nanomaterials) have shown encouraging results in many animal studies, their potential long-term toxicity remains a concern that hampers the clinical translation of those nano-agents [23-28]. Recently, conjugated polymers such as polyaniline [29], polypyrrole (PPy) [30, 31], and poly (3, 4-ethylenedioxythiophene): poly (styrenesulfonate) (PEDOT: PSS) [32] with strong NIR absorption have also attracted much attention as photothermal agents as well as NIR-responsive drug delivery platforms [33]. However, the degradation behaviors of those synthetic conjugated polymers are still not fully understood. More recently, as a natural-inspired conjugated polymer, eumelanin-liked polydopamine (PDA), has been found to be an appealing material for biomedical applications [34, 35]. In 2013, Liu et al. prepared PDA nanoparticles and found them to be a photothermal agent useful for cancer therapy [36]. More recently, Cheng group developed a multifunctional imaging probe with melanin, which has similar structure to PDA, for positron emission tomography (PET) and magnetic resonance (MR) imaging, attributing to its excellent chelating ability with  $^{64}\text{Cu}^{2+}$  and  $\text{Fe}^{3+}$ , respectively [37]. Besides, attributing to its  $\pi$ -conjugated structures, PDA nanoparticles have also been explored as an efficient platform for the loading of various aromatic drugs for cancer therapy [35]. However, the photothermal performance of PDA nanoparticles, which showed a relatively low mass-extinction coefficient in the NIR region, may not be that optimal to be used in PTT. Moreover, the use of PDA nanoparticles as the

platform for imaging-guided chemo-photothermal combination therapy of cancer has not yet been demonstrated to our best knowledge.

Herein, in our system, a safe multifunctional nanopatform is fabricated based on PDA nanoparticles, which are synthesized by oxidation-induced self-polymerization of dopamine in an alkaline environment [38]. The US food and drug administration (FDA)-approved NIR dye ICG is successfully loaded onto PDA nanoparticles, which are then conjugated with a polyethylene glycol (PEG)-grafted amphiphatic polymer to obtain nanoparticles with great physiological stability. Compared with free ICG molecules, ICG in PDA-ICG-PEG nanocomplexes shows red-shifted absorbance peak moved from 780 nm to 800 nm, and exhibits obviously enhanced photostability. By means of  $\pi$ - $\pi$  stacking and hydrophobic interactions, aromatic drug doxorubicin (DOX) can be successfully loaded onto PDA-ICG-PEG nanoparticles with a high loading capacity up to 150% (DOX/PDA, w/w). Moreover, because of the existence of residual phenolic hydroxyl groups on the PDA surface, manganese ions ( $\text{Mn}^{2+}$ ) can be efficiently chelated, offering a strong contrast in T1-weighted MR imaging. By utilizing the PDA-ICG-PEG/DOX (Mn) as the theranostic agent, we observe a great in vivo synergistic therapeutic effect via the MR imaging-guided chemo- & photothermal combination therapy, which in the meantime renders little side effect to the treated animals. This work demonstrates that our PDA nanoparticles, which exhibit similar molecular structures to endogenous biomaterial of melanin, could be a versatile platform for loading of multiple therapeutic and imaging agents, promising for cancer theranostics.

## Result and discussion

The strategy for the fabrication of PDA-ICG-PEG/DOX (Mn) nanocomplexes is illustrated in **Figure 1a**. Water-soluble PDA nanoparticles were firstly synthesized by oxidation and self-polymerization of dopamine monomer in an alkaline solution at pH 8.5. Owing to the amino groups existing on the surface of PDA nanoparticles, they showed positive charges in the acidic solution (isoelectric point  $\approx 4.6$ , **Supplementary Figure S1**). Thus at the pH of 2~3, NIR dye ICG with negative charges could be easily adsorbed on the surface of PDA, likely by both electrostatic and hydrophobic interactions. Afterwards, the obtained PDA-ICG nanocomplexes were washed several times by deionized water to removed excess ICG. To improve the stability of those nanoparticles, which showed increased hydrophobicity on their surface after ICG

loading, an amphiphilic polymer PEG grafted poly(maleic anhydride-alt-1-octadecene) ( $C_{18}$ PMH-PEG) was introduced to modify PDA-ICG. The yielded PDA-ICG-PEG nanoparticles showed uniform sizes as observed by transmission electron microscope (TEM) (Figure 1b). The dynamic light scattering measurement (Figure 1c) showed the hydrodynamic sizes before and after PEGylation to be  $\sim 112$  nm and  $\sim 129$  nm, respectively. Compared to bare PDA nanoparticles, a strong absorption peak centered at  $\sim 800$  nm appeared in the NIR region

(Figure 1d), suggesting that ICG molecules were successfully integrated with PDA. Notably, after ICG was adsorbed on PDA nanoparticles, its absorbance showed an obvious red-shift from 780 nm to 800 nm, which would be preferred for photothermal heating with the commonly used NIR laser at 808-nm. Those PEGylated PDA-ICG (PDA-ICG-PEG) nanoparticles showed excellent stability in water, NaCl and PBS solutions (Inserted pictures in Figure 1d), without any precipitate after 24 h.

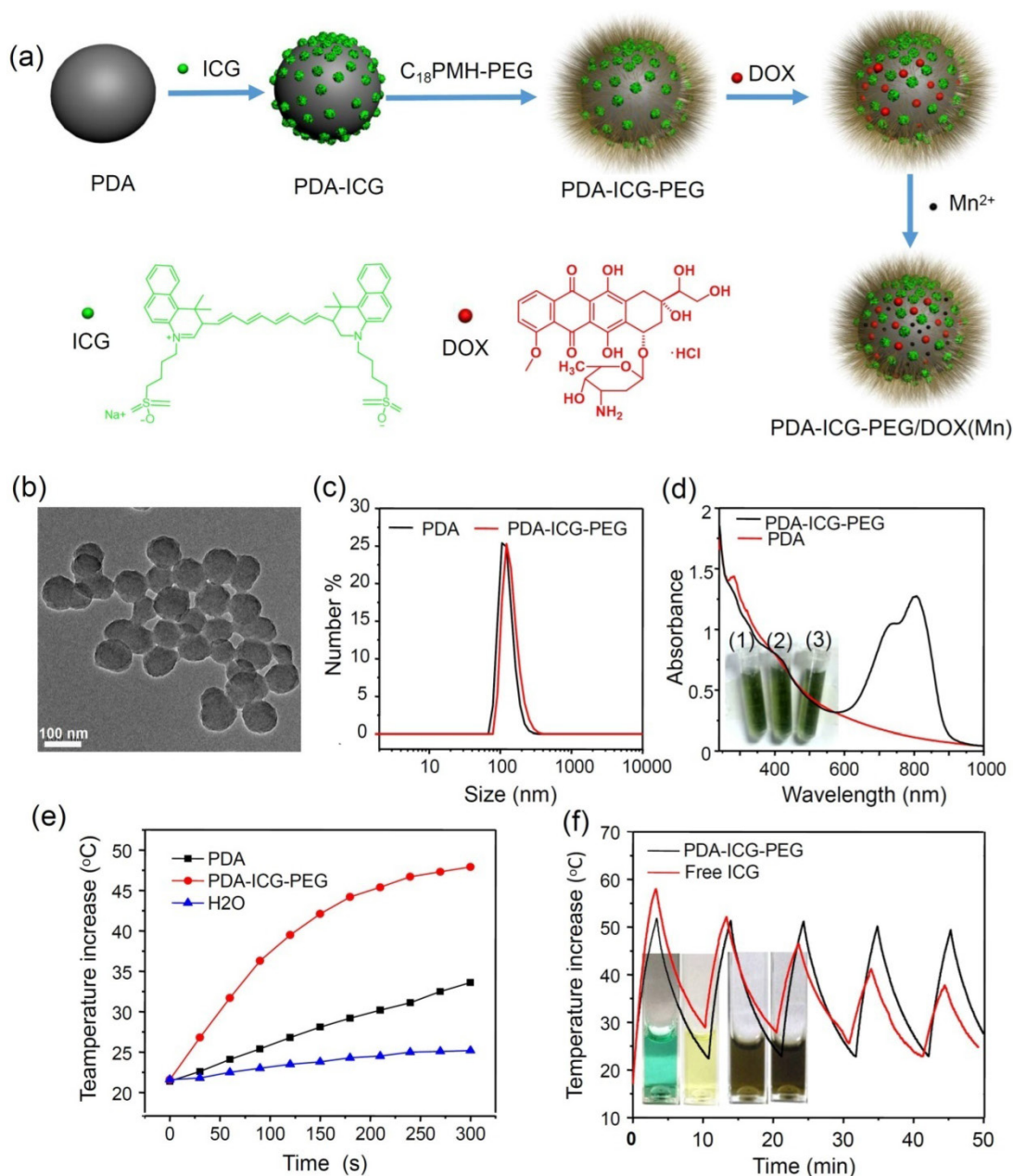


**Figure 1.** Preparation and characterization of PDA-ICG-PEG. (a) A scheme showing the synthesis of PDA-ICG-PEG nanoparticles, as well as the followed drug loading and metal ion chelating. (b) A TEM image of PDA-ICG-PEG nanoparticles. (c) Dynamic light scattering (DLS) data of PDA and PDA-ICG-PEG nanoparticles in aqueous solutions. (d) UV-Vis-NIR spectra of PDA and PDA-ICG-PEG. Inset: a photo of PDA-ICG-PEG in different solutions: water (1), NaCl (2) and PBS (3). (e) Temperature changes of water, PDA and PDA-ICG-PEG at same PDA concentrations (0.014 mg/ml) under irradiation by the 808-nm laser (0.8 W/cm<sup>2</sup>). (f) Temperature changes of PDA-ICG-PEG and free ICG solutions with the same ICG concentration under irradiation of the 808-nm laser with the power density of 0.8 W/cm<sup>2</sup> for 5 cycles (3 min of irradiation for each cycle). Inset: Photos of free ICG and PDA-ICG-PEG solutions before (left) and after (right) laser irradiation.

PDA nanoparticles have been used as a photothermal agent in recent years [39]. However, owing to the relatively low NIR absorbance of PDA, to achieve a desired temperature increase may need high concentrations of PDA or high laser power densities during PTT. ICG as a FDA approved NIR dye has also been used as a photothermal agent [40-42]. However, free ICG molecules suffer from serious photo-bleaching after being exposed to the NIR laser [43, 44]. In our system, with the same concentration of PDA (0.014 mg/mL), the temperature of PDA nanoparticles could only increase by 11°C after NIR laser irradiation (0.8 W/cm<sup>2</sup>, 5 min), whereas the PDA-ICG-PEG solution could be quickly heated up with a temperature increase by 26°C under the same irradiation parameter (**Figure 1e**), demonstrating the remarkably enhanced photothermal conversion efficiency for ICG-loaded nanoparticles. On the other hand, compared with free ICG, our PDA-ICG-PEG nanoparticles showed much better photostability. As shown in **Figure 1f**, after 5 cycles of irradiation by an 808-nm laser at 0.8 W/cm<sup>2</sup> (3 min for each cycle), the photothermal heating efficiency of free ICG declined rapidly, in marked contrast to PDA-ICG-PEG, whose photothermal heating ability remained robust after 5 cycles of laser exposure. Different from free ICG which lost its color and NIR absorbance after repeated laser irradiation (inserted pictures in **Figure 1f**), PDA-ICG-PEG exhibited greatly enhanced stability under photothermal heating (**Supplementary Figure S2**). Moreover, while free ICG would gradually aggregate in the aqueous solution and show broadened / red-shifted NIR absorbance[45], PDA-ICG-PEG exhibited much better stability as evidenced by the largely unchanged absorbance spectrum even after a long period of storage (**Supplementary Figure S3a, S3b**).

The above observed optical properties of PDA-ICG-PEG may be explained by the controlled assembly of ICG molecules on nanoparticles, so that the delocalized electrons between ICG molecules would lead to the red-shifted absorbance peak. In the meanwhile, the reduced interaction between ICG and surrounding water / oxygen molecules after loading on nanoparticles may be helpful to reduce its photo-bleaching. Moreover, the stabilized packing of ICG on PDA nanoparticles could prevent further aggregation of ICG molecules. Therefore, those properties make PDA-ICG-PEG nanocomplexes to be an effective photothermal agent with improved performances compared with bare PDA nanoparticles or free ICG.

It is known that aromatic molecules can be effectively loaded on nanoparticles with delocalized

$\pi$ -electrons by  $\pi$ - $\pi$  stacking and hydrophobic interaction [46, 47]. Since PDA also contains delocalized  $\pi$ -electron structures, we wondered whether PDA-ICG-PEG could also act as a NDDS to load a commonly used chemotherapy drug, doxorubicin (DOX). In our experiments, PDA-ICG-PEG was mixed with DOX at different ratios and incubated in the phosphate buffer (PB) (20 mM, pH=8.0) overnight. After washing with deionized water for several times, the obtained PDA-ICG-PEG/DOX nanocomplexes were then detected by UV-Vis-NIR spectrum (**Figure 2a, Supplementary Figure S4**). A characteristic absorption peak of DOX at 490 nm was observed, indicating the successful loading of DOX on those nanoparticles. Besides, the fluorescence of DOX was quenched by 92% after loading on nanoparticles compared with same concentration of free DOX, also suggesting the strong interaction between DOX and PDA-ICG-PEG (**Supplementary Figure S5**). With the increase of feeding DOX: PDA weight ratios, the drug loading on nanoparticles also increased (**Figure 2b**). The maximal loading capacity reached to ~150% (DOX: PDA, w/w), which appears to be much higher than conventional polymer-based NDDSs.

Next, we studied the drug release behaviors of our DOX loaded on nanoparticles. To study the pH-dependent drug release, the released DOX was collected by dialyzing PDA-ICG-PEG/DOX in PB (20 mM) with different pH values (5.0 and 7.4) (**Figure 2c**). The amount of released DOX was analyzed by UV-Vis-NIR spectrum. 24 h later, about 41.8% of DOX released from nanoparticles under pH 5.0, in contrast to only 15.7% of DOX released under pH 7.4. Such acid-triggered release is owing to the protonation of the amino group in the DOX molecule under reduced pH. We then wondered whether NIR-induced photothermal heating could also trigger drug release from nanoparticles. PDA-ICG-PEG/DOX samples in pH 5.0 and 7.4 PB solutions were irradiated by the 808-nm laser (0.8W/cm<sup>2</sup>, 5 min) at different time points. The cumulative release of DOX from PDA-ICG-PEG/DOX was collected and then measured by UV-Vis-NIR spectra (**Figure 2d, Supplementary figure S6a, S6b**). Compared with DOX released in dark without laser irradiation, the DOX release with NIR-stimulus was dramatically enhanced. Moreover, with same laser irradiation, the DOX release at the lower pH value (5.0) seemed to be more obvious compared to that under the physiological pH (7.4). Considering that the acidic microenvironment of endo/lysosomes in tumor cells, while the pH value in the normal physiological conditions and extracellular environment is neutral, the NIR-triggered drug release would be more

effective once nanoparticles are internalized by cells compared to nanoparticles outside cells.

Next, we investigated the cytotoxicity of our nanoparticles with and without drug loading. Murine breast cancer 4T1 cells and human cervical cancer HeLa cells were selected as the evaluation criterion. No obvious toxicity to both cell lines was observed after cells were incubated with different concentrations of PDA-ICG-PEG for 24 h as evidenced by the standard methylthiazolyltetrazolium (MTT) assay (**Figure 3a**). To investigate the chemotherapy effect, PDA-ICG-PEG/DOX and free DOX with different concentrations were incubated with 4T1 cells for 24 h (**Figure 3b**). DOX at both formulations showed similar cytotoxicity to cancer cells.

It has been proven by several reports that a mild hyperthermal treatment (about 43 °C) could easily enhance the uptake of nanoparticles or drugs [48, 49]. As the result, a synergetic effect may be obtained when integrating chemotherapy with photothermal treatment. In our system, PDA-ICG-PEG/DOX or free DOX was incubated with 4T1 cells, which were then

immediately exposed to the NIR laser (808 nm, 0.4 W/cm<sup>2</sup>, 20 min). After irradiation, the cells were thoroughly washed with PBS for several times to remove non-internalized drugs or nanoparticles. The cells were then imaged by a confocal fluorescence microscope (**Figure 3c**). It was found that cells incubated with free DOX with or without laser irradiation showed no difference in DOX fluorescence intensity. Exhilaratingly, compared with PDA-ICG-PEG/DOX without laser irradiation, higher DOX fluorescence signals in nanoparticle-treated cells could be detected after laser irradiation, indicating more DOX-loaded nanoparticles were engulfed by 4T1 cells upon NIR-induced photothermal heating. Flow cytometer data quantitatively confirmed the above results (**Supplementary Figure S7a-b**). Therefore, similar to previous findings, a mild photothermal heating could easily trigger the cell membrane permeability enhancement, thus increasing the intracellular delivery of drug-loaded nanoparticles [50].

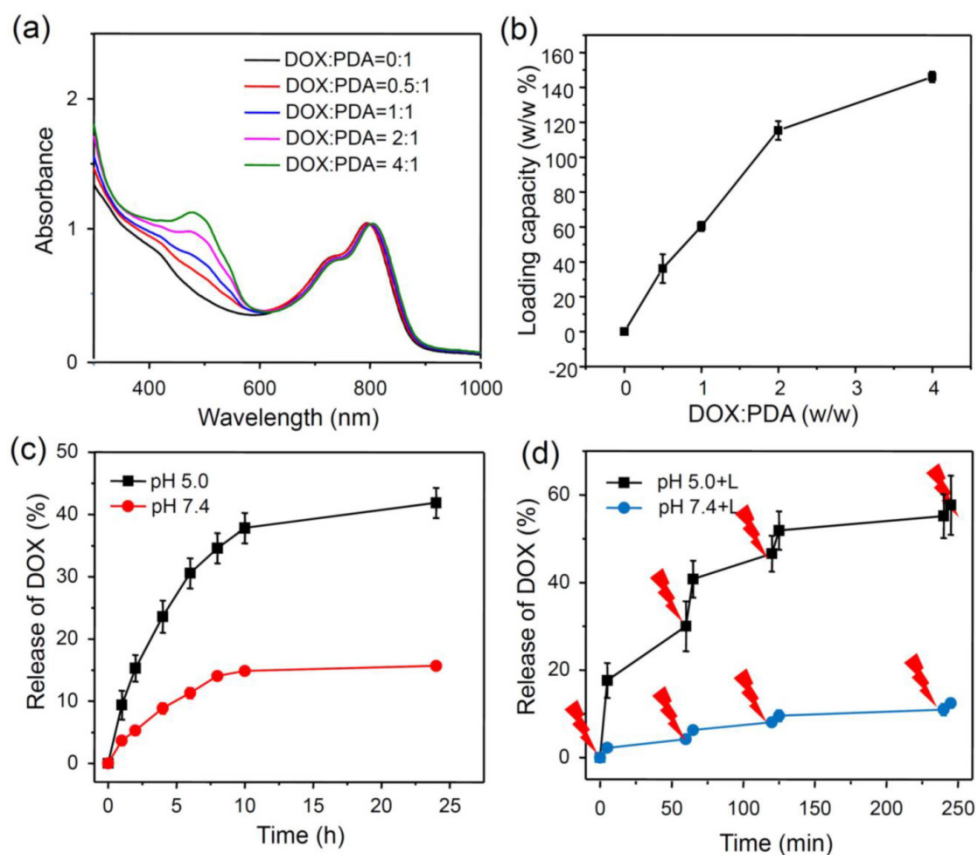


**Figure 2.** Drug loading and release. (a) UV-Vis-NIR spectra of DOX loaded PDA-ICG-PEG with different feeding ratios of DOX to PDA. (b) Quantification of DOX loading at different DOX : PDA ratios. (c) DOX release from PDA-ICG-PEG-DOX nanoparticles in buffers at the different pH values. (d) NIR-triggered release of DOX from PDA-ICG-PEG-DOX nanoparticles. The samples were irradiated with an NIR laser (0.8 W/cm<sup>2</sup>) for 5 min at different time points as indicated by the arrows. Error bars were based on at least triplicated measurements.

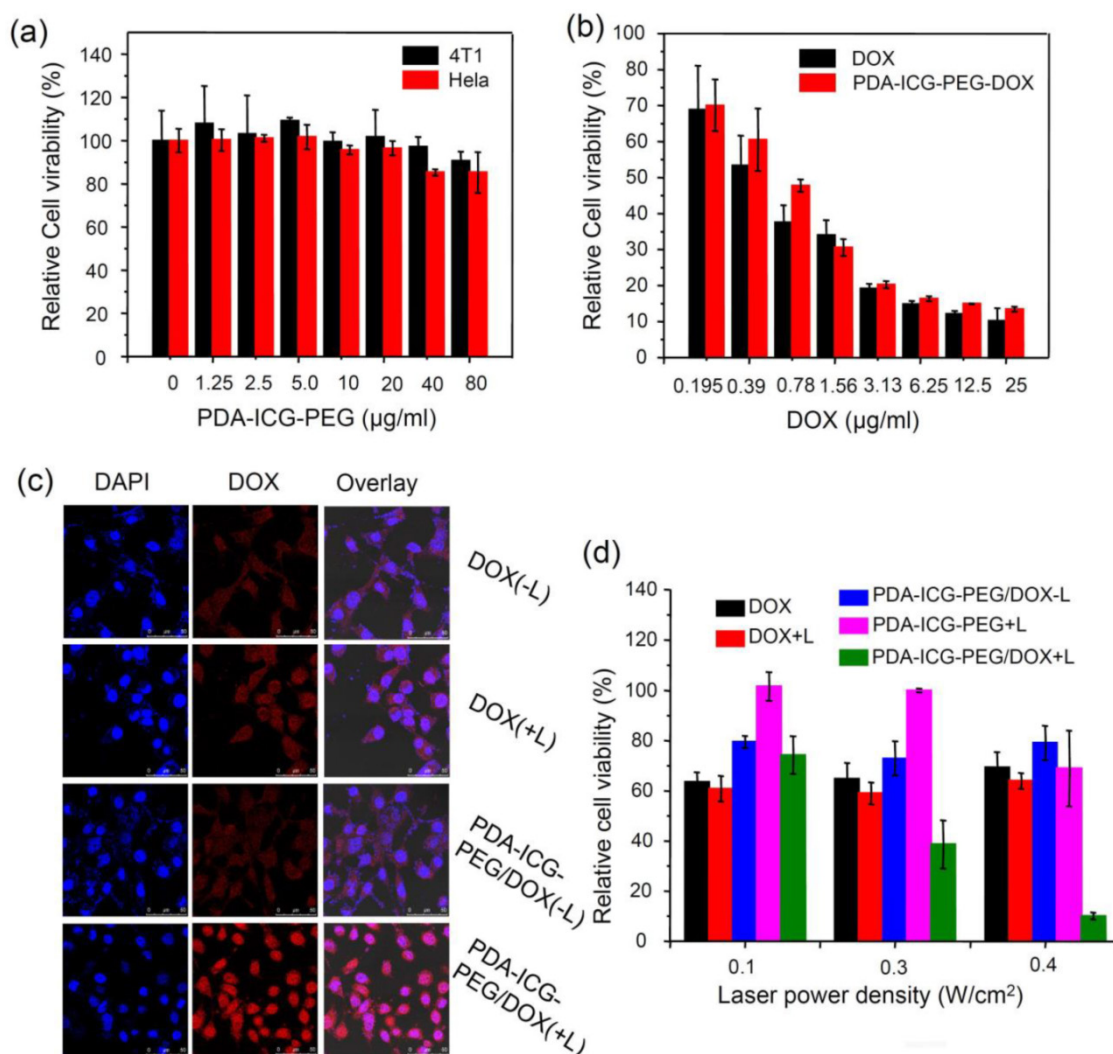


**Figure 3.** In vitro combination therapy. (a) Relative viabilities of 4T1 cells and HeLa cells after being incubated with various concentrations of PDA-ICG-PEG for 24 h. (b) Relative viabilities of 4T1 cells after being incubated with free DOX or PDA-ICG-PEG/DOX at various concentrations for 24 h. (c) Confocal fluorescence images of 4T1 cells incubated with PDA-ICG-PEG/DOX (or free DOX) with/without laser irradiation (808 nm, 0.8 W/cm<sup>2</sup>, 20 min). (d) Relative viabilities of 4T1 cells after being incubated with DOX, PDA-ICG-PEG, PDA-ICG-PEG/DOX with/without laser irradiation at different power density for 20 min. The cell viability test was conducted after further incubation for 24 h. The data are shown as mean  $\pm$  standard deviation (SD) with at least triplicated measurements.

For in vitro combination therapy, 4T1 cells were incubated with free DOX, PDA-ICG-PEG and PDA-ICG-PEG/DOX and then irradiated by the 808-nm laser at different power densities for 20 min (0.1, 0.3, 0.4 W/cm<sup>2</sup>). Excess nanoparticles or drugs were washed with fresh cell medium. Then standard MTT assay was conducted after 24 h. As shown in **Figure 3d**, 4T1 cells incubated with PDA-ICG-PEG/DOX and then irradiated by 808-nm laser showed remarkably reduced viabilities as the laser power densities increased from 0.1 to 0.4 W/cm<sup>2</sup>. However, the single chemotherapy group which treated with free DOX at the same conditions (short incubation time) showed little cytotoxicity, and was not affected by laser exposure. On the other hand, the photothermal effect by PDA-ICG-PEG, without chemotherapy, was also not as effective compared with the combined therapy. Thus, our results

demonstrated the enhanced cell killing synergistic effect by combined chemo- & photothermal therapy based on PDA-ICG-PEG nanoparticles as the drug loading nanoplatform.

It is known that the phenolic hydroxyl group can easily chelate different kinds of metal ions, such as Fe<sup>3+</sup>, Zn<sup>2+</sup>, Cu<sup>2+</sup> and Mn<sup>2+</sup> ions [34]. Among those metal ions, Mn<sup>2+</sup> has been widely used as a contrast agent for magnetic resonance (MR) imaging [51, 52]. Based on our system, Mn<sup>2+</sup> was successfully loaded in a mild condition by intrinsically chelating with phenolic hydroxyl groups in PDA. Interesting, the obtained PDA-ICG-PEG/DOX(Mn) showed obvious concentration-dependent brightening effect under T1-weighted MR imaging, as well as darkening effect under T2-weighted MR imaging (**Figure 4a-c**). The T1 relaxivity (r1) and T2 relaxivity (r2) of PDA-ICG-PEG/DOX (Mn) were measured to be 14.15

$\text{mM}^{-1} \text{s}^{-1}$  and  $39.2 \text{ mM}^{-1} \text{ s}^{-1}$ , respectively. Thus, our Mn-doped PDA nanoparticles could serve as the contrast agent for both T1-weighted and T2-weighted MR imaging.

Before in vivo combination therapy, we firstly examined the behavior of our PDA-ICG-PEG/DOX in vivo. Female Balb/c mice were intravenously (i.v.) injected with PDA-ICG-PEG/DOX(Mn) ([DOX] =  $10 \text{ mg/kg}$ ,  $200 \mu\text{L}$ ). At each time point, the blood was collected from mice. After being dissolved with lysis buffer and extracted with HCl/isopropanol, DOX was detected by fluorescence to determine its concentrations in the blood. As shown in **Supplementary Figure S8**, the DOX signals gradually reduced over time following a two-compartment

model, with the first ( $t_{1/2(\alpha)}$ ) and second ( $t_{1/2(\beta)}$ ) phases of circulation half-lives determined to be  $0.55 \pm 0.12 \text{ h}$  and  $8.53 \pm 0.77 \text{ h}$ , respectively.

Next, in vivo MR image on mice was carried out. Mice bearing 4T1 tumors were firstly i.v. injected with PDA-ICG-PEG/DOX(Mn) and then imaged under a 9.4-T MR imaging system. An obvious brightening effect could be observed in the tumor region at 24 h post injection (p.i.) compared with the pre-injected image (**Figure 4d**). Furthermore, the quantitative MR imaging given by region-of-interest (ROI) quantification also verified the enhancement of T1-weighted MR signals, further evidencing the effective tumor accumulation of those nanoparticles (**Figure 4e**).

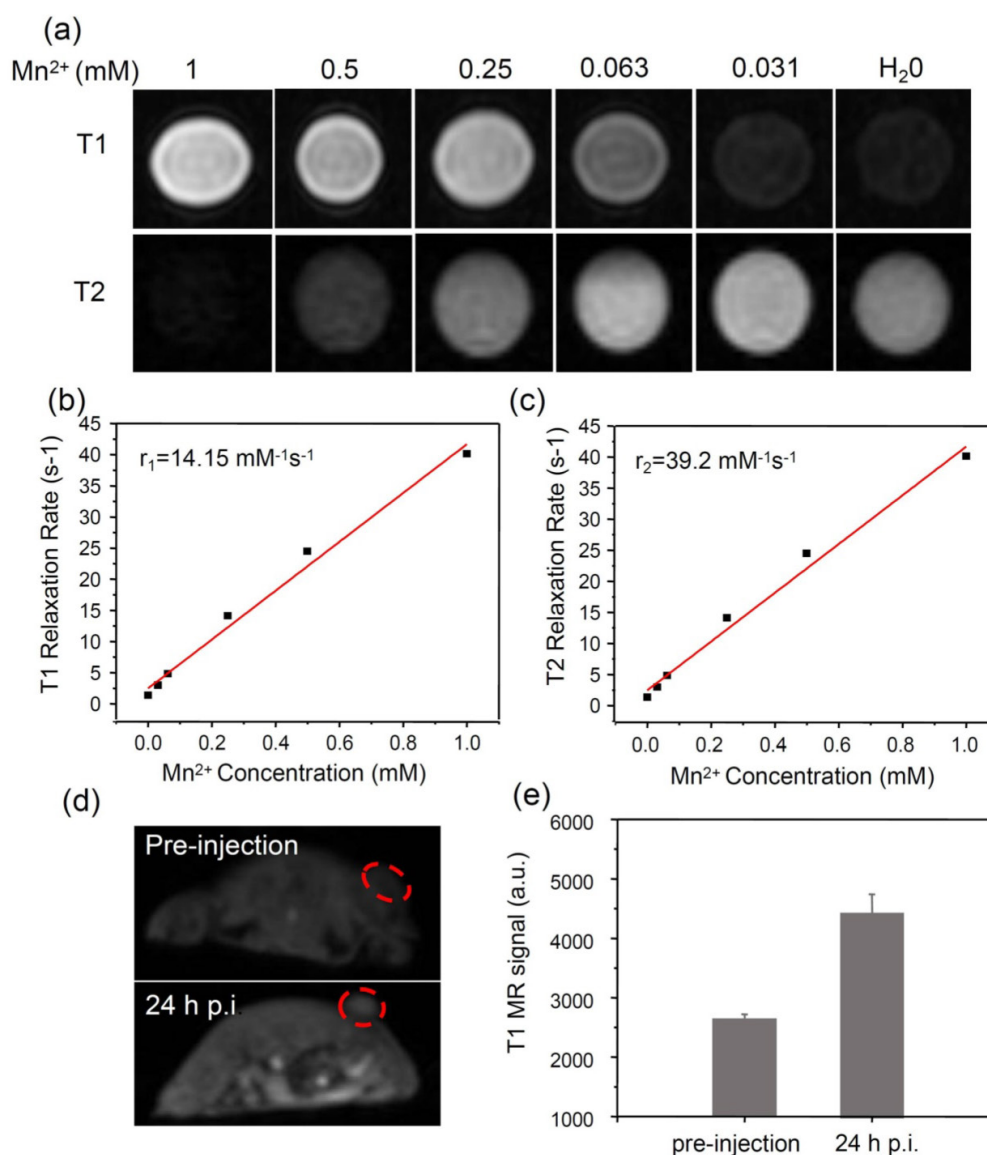


**Figure 4.** MR imaging. (a) T1 and T2 weighted MR images of PDA-ICG-PEG/DOX(Mn) with various  $\text{Mn}^{2+}$  concentrations. (b&c) The T1 relaxation rates (b) and T2 relaxation rates (c) of PDA-ICG-PEG/DOX(Mn) aqueous solutions with different  $\text{Mn}^{2+}$  concentrations. The longitudinal relaxivity ( $r_1$ ) and transverse relaxivity ( $r_2$ ) were determined to be  $14.15 \text{ mM}^{-1} \text{ s}^{-1}$  and  $39.2 \text{ mM}^{-1} \text{ s}^{-1}$ , respectively. (d) In vivo T1-weighted MR images of mouse taken before injection (upper) and 24 h post i.v. injection (bottom) with PDA-ICG-PEG/DOX(Mn). A brightening effect could be observed in the tumor region. (e) T1-weighted MR signals in the tumor before injection and 24 h post i.v. injection with PDA-ICG-PEG/DOX(Mn).

Encouraged by the above mentioned *in vivo* imaging results, *in vivo* cancer treatment with PDA-ICG-PEG/DOX was then carried out. Female Balb/c mice were subcutaneously injected with  $1 \times 10^6$  4T1 cells into the back of each mouse. After one week when the tumors grew to  $50 \sim 60 \text{ mm}^3$ , the mice were divided into five groups: (1) PDA-ICG-PEG/DOX, (2) PBS (plus Laser), (3) free DOX (plus Laser), (4) PDA-ICG-PEG (plus Laser), and (5) PDA-ICG-PEG/DOX (plus Laser). The drug and drug-loaded nanoparticles were *i.v.* injected into each mouse through tail vein (dose =  $10 \text{ mg/kg}$  for DOX,  $2.3 \text{ mg/kg}$  for ICG). After 24 h, those mice were irradiated by the 808-nm laser with a power density of  $0.5 \text{ W/cm}^2$  for 20 min. The temperature change during irradiation was monitored by an IR thermal camera (Figure 5a, 5b). The tumor temperature of mice with PDA-ICG-PEG/DOX or PDA-ICG-PEG injection showed rapid increase and maintained at  $46 \text{ }^\circ\text{C}$  during laser irradiation. In contrast, the tumor temperature showed little change for mice injected

with DOX and PBS under laser irradiation with the same parameters.

After laser treatment, the tumor volumes were monitored by digital caliper every two days for two weeks (Figure 5c). The combination therapy group, PDA-ICG-PEG/DOX with laser irradiation, showed significantly inhibited growth of tumors. In fact, 4 out of 5 tumors in this group were completely eliminated after treatment. PDA-ICG-PEG with laser irradiation had a slight inhibitory effect in the early several days, but grew normally later on. The remaining three treatment groups seemed to have no effect on tumor growth. Slices of tumors with hematoxylin and eosin (H&E) staining were obtained to further verify the therapeutic effect after various treatments (Figure 5d). It was found that much higher damage appeared in the combination treatment group (PDA-ICG-PEG/DOX with laser irradiation), whereas the other four groups showed little or no damage on tumor cells, which had the normal membrane morphology and nuclear structures.

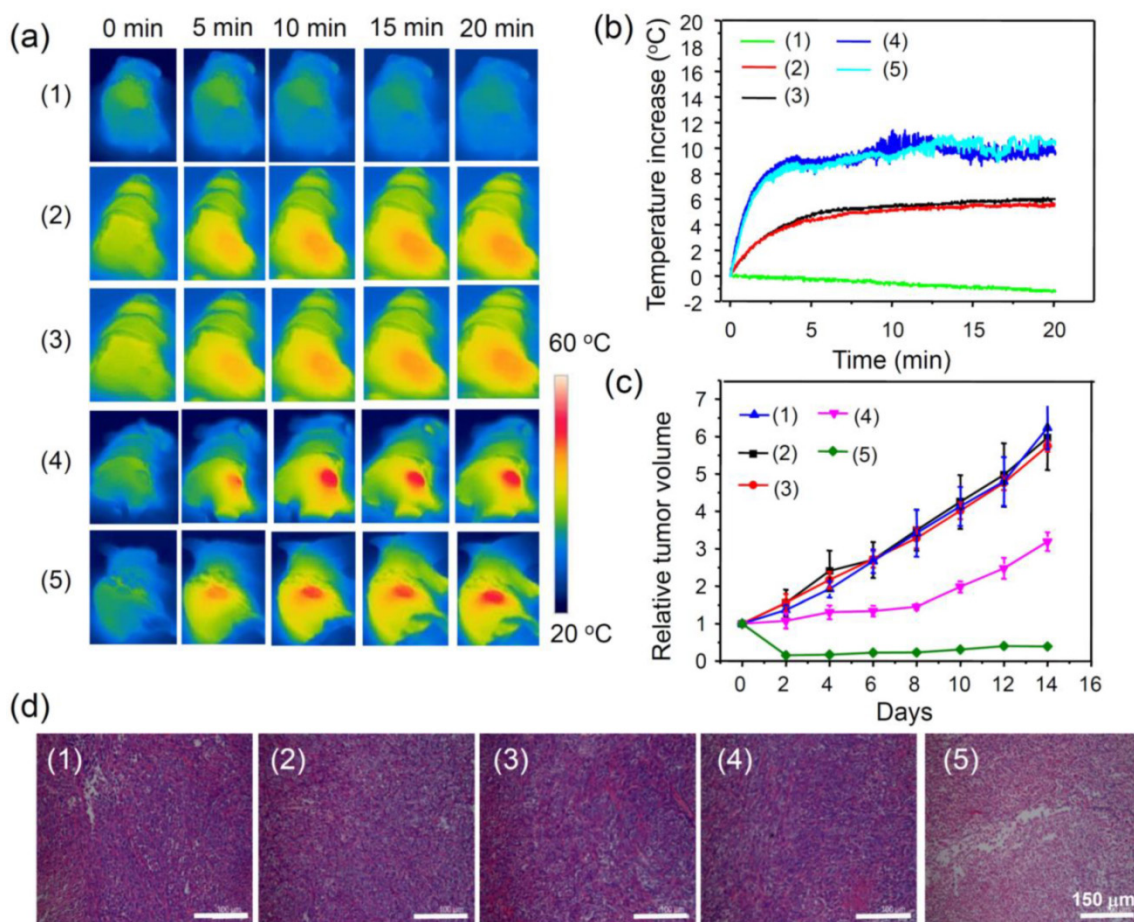


**Figure 5.** *In vivo* combination therapy. (a) IR thermal images of 4T1 tumor-bearing mice with/without the NIR laser irradiation ( $808 \text{ nm}$ ,  $0.5 \text{ W/cm}^2$ , 20 min) after *i.v.* injection with PBS, free DOX, PDA-ICG-PEG, PDA-ICG-PEG/DOX for 24 h at the same PDA and DOX concentrations. (b) Temperature changes of tumor-bearing mice monitored by the IR thermal camera in different groups during laser irradiation as indicated in (a). (c) Tumor growth curves of different groups of mice (5 mice for each group) after various treatments indicated in (a). (d) H&E stained slices of tumors collected from mice one day after various treatments indicated. Note: (1), (2), (3), (4), (5) were used to represent, PDA-ICG-PEG/DOX (1), PBS (plus Laser) (2), free DOX (plus Laser) (3), PDA-ICG-PEG (plus Laser) (4), and PDA-ICG-PEG/DOX (plus Laser) (5).

At last, the average body weights, which were recorded along with tumor volume, showed little change with various treatments after combination therapy (**Supplementary Figure S9**). The slices collected from major organs of control group (PBS) and combination group (PDA-ICG-PEG/DOX +Laser) after two weeks also showed no appreciable organ damage (**Supplementary Figure S10**). Those experimental results clarified the negligible toxicity of our materials. Not surprisingly, PDA, which has the similar structure with melanin existing in living organism, certainly owns the excellent biocompatibility, and can be used as a safe nanopatform for cancer theranostics.

## Conclusions

In summary, we have fabricated a new multifunctional nanopatform based on natural inspired PDA nanoparticles for imaging-guided combination cancer therapy. In this work, PDA showed great biocompatibility and multifunctional molecular loading properties. ICG as a photothermal agent was absorbed by electrostatic interaction with PDA, obtaining ICG loaded PDA which showed greatly enhanced photothermal conversion efficiency compared with free PDA nanoparticles, as well as better photostability compared with free ICG. In the meanwhile, DOX could be loaded on to PDA-ICG-PEG nanoparticles by  $\pi$ - $\pi$  stacking and hydrophobic interaction with high efficiency for chemotherapy. In addition, chelation with  $Mn^{2+}$  ions further offered those nanoparticles great contrasts in MR imaging. Thus, with those functional parts combined, imaging-guided cancer combination therapy was demonstrated in our mouse tumor model experiments, achieving a remarkable synergistic effect in destructing tumors after the photothermal-chemotherapy delivered by PDA-ICG-PEG/DOX. Compared with other types of theranostic inorganic and organic NDDSs, such PDA-based nano-platfom shows a number of unique advantages including great biocompatibility, easy and cost-effective fabrication, as well as the capability to load various imaging and therapeutic molecules with high efficiencies.

## Experimental section

### Materials

Dopamine hydrochloride and Indocyanine green were purchased from Sigma-Aldrich, sodium hydroxide (NaOH), sodium chloride (NaCl), hydrochloric acid (HCl) and Tris (hydroxymethyl) aminomethane were obtained from Sinopharm Chemical Reagent CO, Ltd., China.  $NH_2$ -mPEG (5k)

was obtained from Peg Bio, Suzhou, China. Doxorubicin (DOX) was bought from Beijing Hua Feng United Technology Co. Ltd. All aqueous solution used in experiment was deionized water (18.2 M $\Omega$ .cm) obtained from Milli-Q water purification system.

### Synthesis of PDA-ICG nanoparticles

To obtain PDA-ICG, 180 mg of dopamine (DA) was dissolved in 90 mL deionized water, into which 1 M NaOH solution was added. After 5 h of oxidation and self-polymerization under magnetic stirring, the obtained dark grey polydopamine (PDA) nanoparticles were centrifuged (14800 rpm) and washed with deionized water for three times. After then, the pH value of this PDA solution (2ml, 1 mg/mL) was adjusted to 2~3. Afterwards, indocyanine green (ICG) solution (1ml, 0.5 mg/mL) was mixed with PDA under ultrasonic condition. After stirring for 2 h and centrifuging for several times to remove excess ICG, PDA-ICG nanoparticles were obtained.

### PEGylation of PDA-ICG nanoparticles

To stabilize PDA-ICG, an amphiphilic polymer  $C_{18}$ PMH-PEG was introduced, which was synthesized following our previous protocol [30].  $C_{18}$ PMH-PEG modified PDA-ICG was prepared by mixing 10 mg PDA-ICG nanoparticles and 50 mg  $C_{18}$ PMH-PEG under ultrasonic condition for 12 hand then stirring overnight. The above solution was purified by centrifugation and then wished with DI water for 3 times to remove excess  $C_{18}$ PMH-PEG. The as-obtained PDA-ICG-PEG was re-dispersed in water for following use.

### Doxorubicin loading and releasing

PDA-ICG-PEG (1 mg/mL) was firstly dissolved in phosphate buffer (20 mM) at pH 8.0. Then, DOX at different weight ratios with PDA-ICG-PEG (DOX: PDA =0.5, 1, 2 and 4) was added. After stirring overnight in the dark, the above solutions were centrifuged and washed with PB solutions until the supernatant is colorless. The DOX loading capacity was detected by UV-Vis-NIR spectra. Drug release at pH 5.0 and 7.4 was then investigated by collecting the released free DOX from dialysate for different periods of time. The concentrations of DOX released from PDA-ICG-PEG/DOX were also measured by UV-Vis-NIR spectra.

NIR-simulated release of DOX was carried out by 808-nm laser irradiation. In a typical experiment, the PDA-ICG-PEG/DOX was dissolved in 5 mL PB solution at different pH values (5.0 and 7.4). At different time points, the samples were irradiated by an 808-nm laser for 5 min with the power density of

0.75 W/cm<sup>2</sup>. After treatment, 500  $\mu$ L of solution was collected and centrifuged to obtain released DOX, which was measured and determined by UV-Vis-NIR spectrum.

### Preparation of Mn<sup>2+</sup> chelated PDA-ICG-PEG/DOX

The PDA-ICG-PEG/DOX nanocomplexes (1 mg/mL) were labeled with Mn<sup>2+</sup> by adding of MnCl<sub>2</sub> solution (1 mg/mL) at the neutral condition. After 4 h stirring at 40°C, the samples were centrifuged for several times to remove unbound excess Mn<sup>2+</sup>. The concentration of Mn<sup>2+</sup> in the obtained nano-complexes was measured by inductively coupled plasma-mass spectrometry (ICP-MS) analysis.

### Cellular experiments

4T1 cells and HeLa cells were purchased from American Type Culture Collection (ATCC) and cultured under standard conditions (37°C, 5% CO<sub>2</sub>). To determine the cytotoxicity of nanocomplexes, 4T1 and HeLa cells were seeded in 96-well plates with 1×10<sup>4</sup> cells/well. Then, different concentrations of PDA-ICG-PEG, PDA-ICG-PEG/DOX and free DOX were added and co-incubated with cells for 24 h. Afterwards, the cells were washed with free cell culture medium for twice. The relative cell viabilities compared with untreated groups were measured by the MTT assay.

To test the NIR-triggered cell uptake of nanoparticles, 4T1 cells were seeded in 12-well plates. Then, PDA-ICG-PEG/DOX or free DOX with same concentration of DOX ([DOX] = 25  $\mu$ M) was added. Immediately, the cells were irradiated with / without 808-nm laser for 20 min at the power density of 0.4 W/cm<sup>2</sup>. The above cells were then washed with PBS three times to remove excess drugs or nanoparticles. The cell uptake of DOX was determined by confocal images (Lecia SP5II laser scanning confocal microscope) by recording DOX fluorescence. Meanwhile, with trypsin treatment, the cells were analyzed by flow cytometer (Calibur, BD Biosciences, USA).

For in vitro combination therapy, 4T1 cells in 96-well plates were incubated with PDA-ICG-PEG/DOX, PDA-ICG-PEG/DOX (Plus Laser), PDA-ICG-PEG (Laser), free DOX (-Laser) and free DOX (+Laser), with the same concentration of DOX ([DOX] = 25  $\mu$ M). Then, the cells were / were not irradiated by 808-nm laser with power densities at 0.1, 0.3 and 0.4 W/cm<sup>2</sup> for 20 min. Afterwards, the cells were washed by fresh cell medium for three times and incubated for 24 h, before the cell viability MTT assay.

### Mouse tumor model

In our experiments, female BaLb/c mice were

purchased from Nanjing Peng Sheng Biological Technology Co, Ltd. Animal experiments were performed following protocols approved by Soochow University Laboratory Animal Center. To develop the tumor model, 4T1 cells (1×10<sup>6</sup>) in 50  $\mu$ L PBS were subcutaneously injected into the back of each mouse. After about one week, the average size of tumor was about 60 mm<sup>3</sup>.

For in vivo combination therapy, 4T1 tumor-bearing mice were divided into five groups, PDA-ICG-PEG/DOX (1), PBS (plus Laser) (2), free DOX (plus Laser) (3), PDA-ICG-PEG (plus Laser) (4), and PDA-ICG-PEG/DOX (plus Laser) (5). In each group, 200  $\mu$ L of materials at the same concentration of DOX (10 mg/kg) and PDA (10 mg/kg) were intravenously injected. After 24 h, the tumors were irradiated by the 808-nm laser for 20 min at the power density of 0.5 W/cm<sup>2</sup>. During the laser irradiation, the temperature change of tumors was recorded by an Infrared thermal imaging camera (ICI 7320). After treatment, the size change of tumor was monitored by digital caliper to record the lengths and widths every two days for two weeks. The tumor volumes were calculated by "length X width<sup>2</sup>/2".

### Blood circulation

200  $\mu$ L of PDA-ICG-PEG/DOX was i.v. injected into three mice. At each time point, 20  $\mu$ L of blood was collected from the mouse and then dissolved in 300  $\mu$ L of lysis buffer (1% SDS, 1% Triton-100, 40 mM Tris acetate, 10 mM EDTA and 10 mM DTT). To extract DOX from blood, 300  $\mu$ L of HCl/isopropanol was added. Then, the mixture was incubated in dark overnight. By centrifuging to obtain the DOX in supernatant, the amount of DOX remaining in blood was determined by fluorescence.

### MR images

PDA-ICG-PEG/DOX (Mn) dissolved in DI water with different concentrations were scanned by a 3 T clinical MRI scanner (Bruker Biospin Corporation, Billerica, MA, USA). T1 weighted animal MR imaging were performed under the same MR scanner with a special coil designed for small-animal imaging.

### Supplementary Material

Supplementary figures.

<http://www.thno.org/v06p1031s1.pdf>

### Acknowledgments

This work was partially supported by the National 973 Programs of China (2012CB932600), the National Natural Science Foundation of China (51525203, 51222203), a Project Funded by the Priority Academic Program Development of Jiangsu Higher

Education Institutions and a Jiangsu Natural Science Fund for Distinguished Young Scholars.

## Competing Interests

The authors have declared that no competing interest exists.

## References

- Coates A, Abraham S, Kaye SB, Sowerbutts T, Frewin C, Fox RM, et al. On the receiving end – patient perception of the side-effects of cancer chemotherapy. *Eur J Cancer and Clin Oncol*. 1983; 19: 203-8.
- Lage H. An overview of cancer multidrug resistance: a still unsolved problem. *Cell Mol Life Sci*. 2008; 65: 3145-67.
- Min KH, Park K, Kim Y-S, Bae SM, Lee S, Jo HG, et al. Hydrophobically modified glycol chitosan nanoparticles-encapsulated camptothecin enhance the drug stability and tumor targeting in cancer therapy. *J Control Release*. 2008; 127: 208-18.
- Sonvico F, Mornet S, Vasseur S, Dubernet C, Jaillard D, Degrouard J, et al. Folate-Conjugated Iron Oxide Nanoparticles for Solid Tumor Targeting as Potential Specific Magnetic Hyperthermia Mediators: Synthesis, Physicochemical Characterization, and in Vitro Experiments. *Bioconjugate Chem*. 2005; 16: 1181-8.
- Liu J, Wang C, Wang X, Wang X, Cheng L, Li Y, et al. Mesoporous Silica Coated Single-Walled Carbon Nanotubes as a Multifunctional Light-Responsive Platform for Cancer Combination Therapy. *Adv Funct Mater*. 2015; 25: 384-92.
- Song G, Liang C, Gong H, Li M, Zheng X, Cheng L, et al. Core-Shell MnSe@Bi<sub>2</sub>Se<sub>3</sub> Fabricated via a Cation Exchange Method as Novel Nanotheranostics for Multimodal Imaging and Synergistic Theranostic Therapy. *Adv Mater*. 2015; 27: 6110-7.
- Zhao P, Zheng M, Luo Z, Gong P, Gao G, Sheng Z, et al. NIR-driven Smart Theranostic Nanomedicine for On-demand Drug Release and Synergistic Antitumor Therapy. *Sci Rep*. 2015; 5: 14258.
- Lee H, Hong W, Jeon S, Choi Y, Cho Y. Electroactive Polypyrrole Nanowire Arrays: Synergistic Effect of Cancer Treatment by On-Demand Drug Release and Photothermal Therapy. *Langmuir*. 2015; 31: 4264-9.
- Yang P, Li D, Jin S, Ding J, Guo J, Shi W, et al. Stimuli-responsive biodegradable poly(methacrylic acid) based nanocapsules for ultrasound traced and triggered drug delivery system. *Biomaterials*. 2014; 35: 2079-88.
- Yoon YI, Kwon Y-S, Cho H-S, Heo S-H, Park KS, Park SG, et al. Ultrasound-mediated gene and drug delivery using a microbubble-liposome particle system. *Theranostics*. 2014; 4: 1133.
- Oliveira H, Pérez-Andrés E, Thevenot J, Sandre O, Berra E, Lecommandoux S. Magnetic field triggered drug release from polymersomes for cancer therapeutics. *J Control Release*. 2013; 169: 165-70.
- Hayashi K, Nakamura M, Miki H, Ozaki S, Abe M, Matsumoto T, et al. Magnetically responsive smart nanoparticles for cancer treatment with a combination of magnetic hyperthermia and remote-control drug release. *Theranostics*. 2014; 4: 834.
- Du J-Z, Du X-J, Mao C-Q, Wang J. Tailor-Made Dual pH-Sensitive Polymer-Doxorubicin Nanoparticles for Efficient Anticancer Drug Delivery. *J Am Chem Soc*. 2011; 133: 17560-3.
- Pan Y-J, Chen Y-Y, Wang D-R, Wei C, Guo J, Lu D-R, et al. Redox/pH dual stimuli-responsive biodegradable nanohydrogels with varying responses to dithiothreitol and glutathione for controlled drug release. *Biomaterials*. 2012; 33: 6570-9.
- Gong H, Dong Z, Liu Y, Yin S, Cheng L, Xi W, et al. Engineering of Multifunctional Nano-Micelles for Combined Photothermal and Photodynamic Therapy Under the Guidance of Multimodal Imaging. *Adv Funct Mater*. 2014; 24: 6492-502.
- Song X-R, Wang X, Yu S-X, Cao J, Li S-H, Li J, et al. Co<sub>9</sub>Se<sub>8</sub> Nanoplates as a New Theranostic Platform for Photoacoustic/Magnetic Resonance Dual-Modal-Imaging-Guided Chemo-Photothermal Combination Therapy. *Adv Mater*. 2015; 27: 3285-91.
- Zhao P, Zheng M, Yue C, Luo Z, Gong P, Gao G, et al. Improving drug accumulation and photothermal efficacy in tumor depending on size of ICG loaded lipid-polymer nanoparticles. *Biomaterials*. 2014; 35: 6037-46.
- Yan H, Teh C, Sreejith S, Zhu L, Kwok A, Fang W, et al. Functional Mesoporous Silica Nanoparticles for Photothermal-Controlled Drug Delivery In Vivo. *Angew Chem Int Ed*. 2012; 51: 8373-7.
- Wang M, Mi C-C, Wang W-X, Liu C-H, Wu Y-F, Xu Z-R, et al. Immunolabeling and NIR-Excited Fluorescent Imaging of HeLa Cells by Using NaYF<sub>4</sub>:Yb,Er Upconversion Nanoparticles. *ACS Nano*. 2009; 3: 1580-6.
- Kempen PJ, Greasley S, Parker KA, Campbell JL, Chang H-Y, Jones JR, et al. Theranostic Mesoporous Silica Nanoparticles Biodegrade after Pro-Survival Drug Delivery and Ultrasound/Magnetic Resonance Imaging of Stem Cells. *Theranostics*. 2015; 5: 631.
- Cheng L, Liu J, Gu X, Gong H, Shi X, Liu T, et al. PEGylated WS<sub>2</sub> Nanosheets as a Multifunctional Theranostic Agent for in vivo Dual-Modal CT/Photoacoustic Imaging Guided Photothermal Therapy. *Adv Mater*. 2014; 26: 1886-93.
- Chen Q, Liu X, Chen J, Zeng J, Cheng Z, Liu Z. A Self-Assembled Albumin-Based Nanoprobe for In Vivo Ratiometric Photoacoustic pH Imaging. *Adv Mater*. 2015.
- Ji X, Shao R, Elliott AM, Stafford RJ, Esparza-Coss E, Bankson JA, et al. Bifunctional Gold Nanoshells with a Superparamagnetic Iron Oxide-Silica Core Suitable for Both MR Imaging and Photothermal Therapy. *J Phys Chem C*. 2007; 111: 6245-51.
- Zhou F, Xing D, Ou Z, Wu B, Resasco DE, Chen WR. Cancer photothermal therapy in the near-infrared region by using single-walled carbon nanotubes. *J Biomed Opt*. 2009; 14: 021009-7.
- Wang X, Wang C, Cheng L, Lee S-T, Liu Z. Noble Metal Coated Single-Walled Carbon Nanotubes for Applications in Surface Enhanced Raman Scattering Imaging and Photothermal Therapy. *J Am Chem Soc*. 2012; 134: 7414-22.
- Robinson JT, Tabakman SM, Liang Y, Wang H, Sanchez Casalongue H, Vinh D, et al. Ultrasmall Reduced Graphene Oxide with High Near-Infrared Absorbance for Photothermal Therapy. *J Am Chem Soc*. 2011; 133: 6825-31.
- Liang S, Li C, Zhang C, Chen Y, Xu L, Bao C, et al. CD44v6 Monoclonal Antibody-Conjugated Gold Nanostars for Targeted Photoacoustic Imaging and Plasmonic Photothermal Therapy of Gastric Cancer Stem-like Cells. *Theranostics*. 2015; 5: 970-84.
- Jang B, Park S, Kang SH, Kim JK, Kim S-K, Kim I-H, et al. Gold nanorods for target selective SPECT/CT imaging and photothermal therapy in vivo. *Quant Imaging Med Surg*. 2012; 2: 1.
- Zhou J, Lu Z, Zhu X, Wang X, Liao Y, Ma Z, et al. NIR photothermal therapy using polyaniline nanoparticles. *Biomaterials*. 2013; 34: 9584-92.
- Wang C, Xu H, Liang C, Liu Y, Li Z, Yang G, et al. Iron Oxide @ Polypyrrole Nanoparticles as a Multifunctional Drug Carrier for Remotely Controlled Cancer Therapy with Synergistic Antitumor Effect. *ACS Nano*. 2013; 7: 6782-95.
- Park D, Cho Y, Goh S-H, Choi Y. Hyaluronic acid-polypyrrole nanoparticles as pH-responsive theranostics. *Chem Commun*. 2014; 50: 15014-7.
- Cheng L, Yang K, Chen Q, Liu Z. Organic Stealth Nanoparticles for Highly Effective in Vivo Near-Infrared Photothermal Therapy of Cancer. *ACS Nano*. 2012; 6: 5605-13.
- Song X, Chen Q, Liu Z. Recent advances in the development of organic photothermal nano-agents. *Nano Res*. 2015; 8: 340-54.
- Liu Y, Ai K, Lu L. Polydopamine and Its Derivative Materials: Synthesis and Promising Applications in Energy, Environmental, and Biomedical Fields. *Chem Rev*. 2014; 114: 5057-115.
- Cui J, Yan Y, Such GK, Liang K, Ochs CJ, Postma A, et al. Immobilization and Intracellular Delivery of an Anticancer Drug Using Mussel-Inspired Polydopamine Capsules. *Biomacromolecules*. 2012; 13: 2225-8.
- Liu Y, Ai K, Liu J, Deng M, He Y, Lu L. Dopamine-Melanin Colloidal Nanospheres: An Efficient Near-Infrared Photothermal Therapeutic Agent for In Vivo Cancer Therapy. *Adv Mater*. 2013; 25: 1353-9.
- Lin L-S, Cong Z-X, Cao J-B, Ke K-M, Peng Q-L, Gao J, et al. Multifunctional Fe<sub>3</sub>O<sub>4</sub>@Polydopamine Core-Shell Nanocomposites for Intracellular mRNA Detection and Imaging-Guided Photothermal Therapy. *ACS Nano*. 2014; 8: 3876-83.
- Ju K-Y, Lee Y, Lee S, Park SB, Lee J-K. Bioinspired Polymerization of Dopamine to Generate Melanin-Like Nanoparticles Having an Excellent Free-Radical-Scavenging Property. *Biomacromolecules*. 2011; 12: 625-32.
- Black KCL, Yi J, Rivera JG, Zelasko-Leon DC, Messersmith PB. Polydopamine-enabled surface functionalization of gold nanorods for cancer cell-targeted imaging and photothermal therapy. *Nanomedicine*. 2012; 8: 17-28.
- Zheng M, Yue C, Ma Y, Gong P, Zhao P, Zheng C, et al. Single-Step Assembly of DOX/ICG Loaded Lipid-Polymer Nanoparticles for Highly Effective Chemo-photothermal Combination Therapy. *ACS Nano*. 2013; 7: 2056-67.
- Zheng X, Xing D, Zhou F, Wu B, Chen WR. Indocyanine Green-Containing Nanostructure as Near Infrared Dual-Functional Targeting Probes for Optical Imaging and Photothermal Therapy. *Mol Pharm*. 2011; 8: 447-56.
- Sheng Z, Hu D, Zheng M, Zhao P, Liu H, Gao D, et al. Smart Human Serum Albumin-Indocyanine Green Nanoparticles Generated by Programmed Assembly for Dual-Modal Imaging-Guided Cancer Synergistic Phototherapy. *ACS Nano*. 2014; 8: 12310-22.
- Cheng L, Gong H, Zhu W, Liu J, Wang X, Liu G, et al. PEGylated Prussian blue nanocubes as a theranostic agent for simultaneous cancer imaging and photothermal therapy. *Biomaterials*. 2014; 35: 9844-52.
- Saxena V, Sadoqi M, Shao J. Indocyanine green-loaded biodegradable nanoparticles: preparation, physicochemical characterization and in vitro release. *Inter J Pharm*. 2004; 278: 293-301.
- Saxena V, Sadoqi M, Shao J. Degradation kinetics of indocyanine green in aqueous solution. *J Pharm Sci*. 2003; 92: 2090-7.
- Zhang X, Meng L, Lu Q, Fei Z, Dyson PJ. Targeted delivery and controlled release of doxorubicin to cancer cells using modified single wall carbon nanotubes. *Biomaterials*. 2009; 30: 6041-7.
- Liu Z, Sun X, Nakayama-Ratchford N, Dai H. Supramolecular Chemistry on Water-Soluble Carbon Nanotubes for Drug Loading and Delivery. *ACS Nano*. 2007; 1: 50-6.
- Feng L, Yang X, Shi X, Tan X, Peng R, Wang J, et al. Polyethylene Glycol and Polyethylenimine Dual-Functionalized Nano-Graphene Oxide for Photothermally Enhanced Gene Delivery. *Small*. 2013; 9: 1989-97.

49. Sherlock SP, Tabakman SM, Xie L, Dai H. Photothermally Enhanced Drug Delivery by Ultrasmall Multifunctional FeCo/Graphitic Shell Nanocrystals. *ACS Nano*. 2011; 5: 1505-12.
50. Tian B, Wang C, Zhang S, Feng L, Liu Z. Photothermally Enhanced Photodynamic Therapy Delivered by Nano-Graphene Oxide. *ACS Nano*. 2011; 5: 7000-9.
51. Modo M, Hoehn M, Bulte JWM. Cellular MR imaging. *Mol Imaging*. 2005; 4: 143-64.
52. Miao Z-H, Wang H, Yang H, Li Z-L, Zhen L, Xu C-Y. Intrinsically Mn<sup>2+</sup>-Chelated Polydopamine Nanoparticles for Simultaneous Magnetic Resonance Imaging and Photothermal Ablation of Cancer Cells. *ACS App Mater Inter*. 2015; 7: 16946-52.